Chemistry & Biology
Article

Structural Studies of a Peptide with Immune Modulating and Direct Antimicrobial Activity

Michal Wieczorek,[1,3] Håvard Jenssen,[2,3] Jason Kindrachuk,[2,3] Walter R.P. Scott,[1] Melissa Elliott,[2] Kai Hilpert,[2] John T.J. Cheng,[1] Robert E.W. Hancock,[2] and Suzana K. Straus[1,*]
[1]Chemistry Department, University of British Columbia, 2036 Main Mall, Vancouver, BC V6T 1Z1, Canada
[2]Centre for Microbial Diseases and Immunity Research, University of British Columbia, 2259 Lower Mall Research Station, Vancouver, BC V6T 1Z3, Canada
[3]These authors contributed equally to this work
*Correspondence: sstraus@chem.ubc.ca
DOI 10.1016/j.chembiol.2010.07.007

SUMMARY

The structure and function of the synthetic innate defense regulator peptide 1018 was investigated. This 12 residue synthetic peptide derived by substantial modification of the bovine cathelicidin bactenecin has enhanced innate immune regulatory and moderate direct antibacterial activities. The solution state NMR structure of 1018 in zwitterionic dodecyl phosphocholine (DPC) micelles indicated an α-helical conformation, while secondary structures, based on circular dichroism measurements, in anionic sodium dodecyl sulfate (SDS) and phospholipid vesicles (POPC/PG in a 1:1 molar ratio) and simulations revealed that 1018 can adopt a variety of folds, tailored to its different functions. The structural data are discussed in light of the ability of 1018 to potently induce chemokine responses, suppress the LPS-induced TNF-α response, and directly kill both Gram-positive and Gram-negative bacteria.

INTRODUCTION

Host-defense peptides (HDPs) are short amphiphilic peptides that are ubiquitous in nature, where they are an integral component of the anti-infective defense mechanisms of insects, plants, and highly evolved animal species with more complex immune systems (Bowdish et al., 2005b; Mookherjee et al., 2006a; Scott et al., 2007). They are short cationic peptides, consisting of 12 to ~50 amino acid residues, with a net positive charge of +2 to +9, and a high proportion of hydrophobic residues. Some examples include the human cathelicidin LL-37 (Bowdish et al., 2005a), bovine indolicidin (Bowdish et al., 2005b; Rozek et al., 2000) and bactenecin (Wu and Hancock, 1999b), the ubiquitous α- and β-defensins (Crovella et al., 2005; Dhople et al., 2006; Mygind et al., 2005; Sahl et al., 2005), and the bacterial-produced antimicrobial peptides nisin (Hsueh et al., 2005) and polymyxin B (Hancock, 2001; Zhang et al., 2000b).

HDPs are typically unstructured in solution. However, upon contact with hydrophobic phospholipid bilayers of cell membranes, these peptides characteristically adopt an amphiphilic structure. As such, HDPs can be classified into four broad structural groups: β sheets, α helices, loops, and extended structures (Straus and Hancock, 2006). Investigations of HDP antimicrobial or hemolytic activities have demonstrated that the mode of peptide action involves either modest membrane permeabilization followed by peptide translocation across the membrane and subsequent interaction with cytoplasmic targets, or disruption of the cell membrane and bacterial lysis. When the peptides act by disrupting the membrane, they perturb the physical integrity of the bacterial membrane by thinning or transient poration. Although often regarded as direct antimicrobial agents, natural HDPs often display rather weak or ablated antimicrobial activities under physiological conditions (being antagonized by high mono- and divalent cation concentrations and by polyanions); thus, only those peptides that can directly kill microbes under physiological conditions should be termed antimicrobial peptides. Those that are able to kill microbes through modulation of the immune system (with or without antimicrobial activity) are termed HDPs.

It is increasingly appreciated that the role of HDPs as host-defense molecules may be better represented by their ability to modulate the host immune response via a range of mechanisms (Straus and Hancock, 2006). These include, but are not limited to, the recruitment and/or activation of immune cells, angiogenesis and wound healing, dendritic cell maturation, and controlling inflammation and sepsis. For example, α-defensins located in human neutrophils (Rehaume and Hancock, 2008) attract peripheral T cells found in human blood that express CD4/CD45RA and CD8 antigens and also attract immature dendritic cells (Chertov et al., 2000; Zasloff, 2002). HDPs also exhibit indirect antimicrobial activities and reduce proinflammatory responses through alteration of host-gene expression, chemotactic activities, and inhibition of lipopolysaccharide (LPS) induced proinflammatory cytokine production. It has been demonstrated that these peptides can be expressed either in response to the presence of bacterial LPS or inflammatory mediators such as interleukin (IL)-6 or tumor necrosis factor (TNF)-α (Diamond et al., 1996; Zhang et al., 2000a), although others appear to be constitutive. Also, HDPs can sequester LPS shed from Gram-negative bacteria and/or indirectly antagonize LPS mediated cell signaling, preventing the induction of inflammatory responses which, if left unchecked, can lead to potentially deleterious conditions such as sepsis

(Hancock, 2001). The chemokine-inducing properties of such peptides have been shown to depend absolutely on uptake into eukaryotic cells (Lau et al., 2005; Mookherjee et al., 2009; Nijnik et al., 2010; Yu et al., 2009), with two intracellular receptors recently described (Mookherjee et al., 2009; Yu et al., 2009). These peptides all bear the hallmarks of cell penetrating peptides in carrying a net positive charge (often due to arginine residues) and amphipathicity. Although much is known about how HDPs interact with membranes (see, e.g., Haney et al., 2009; Sitaram et al., 2002), little is known about how HDP structure correlates with the immunomodulatory functions of these peptides.

In recent years, there has been an increased effort to design and develop synthetic peptides, termed innate defense regulatory peptides (IDRs), with enhanced immunomodulatory activities, using natural HDPs as templates. Examples include the peptide Bac2A, a linear derivative of the cathelicidin bactenecin found in bovine neutrophils (Bowdish et al., 2005b; Wu and Hancock, 1999a), the synthetic immunomodulatory peptides IDR-1 (Haney et al., 2009) and IDR-1002 (Nijnik et al., 2010), as well as many others (Avrahami and Shai, 2004; Haney et al., 2009; Porcelli et al., 2006; Strömstedt et al., 2009). Recently, new synthetic peptide libraries have been generated using the quantitative structure-activity relationship (QSAR) methodology (Nijnik et al., 2010). This approach exploits the relationship between higher order sequence motifs or contexts and peptide antimicrobial activity to yield lead peptide candidates with optimized activities (Cherkasov et al., 2009). Recently (H.J. and R.E.W.H., unpublished data) a series of peptides, derived from the base sequence of the 12 amino acid antimicrobial and immunomodulatory peptide Bac2A (Wu and Hancock, 1999a), through point substitutions, scrambling, and deletions were iteratively tested for their ability to stimulate immune responses ex vivo, as monitored through elevation of the cytokine/chemokine profile in human peripheral blood mononuclear cells (PMBCs) and confer protection to bacterial challenge in vivo. Of the many peptides generated, peptide IDR-1018 (VRLIVAVRIWRR; abbreviated here as 1018) was a promising candidate with moderate minimal inhibitory concentrations (MIC), minimal hemolytic activity, and a significant reduction in the LPS induced TNF-α response. Interestingly, of the dozens of peptides generated and tested by us to date, 1018 had the highest effect on the induction of chemokines ex vivo as measured by MCP-1 and MCP-3 expression. Intriguingly, 1018 turned out to be distantly related to Bac2A (Wu and Hancock, 1999a, 1999b) in that 1018 has nearly identical amino acid composition to Bac2A (RLARIVVIRVAR), namely, three Val, four Arg, one Leu, two Ile, one Ala, with one A→W substitution and scrambling of the peptide sequence.

To better understand the structure-function relationships of peptide 1018, we have characterized the structure of this peptide in model membranes consisting of lipids with neutral head groups (zwitterionic dodecyl phosphocholine (DPC) micelles, as an analog) and lipids with a mixture of neutral and negatively charged head groups (phosphatidylcholine/phosphatidylglycerol, model for bacterial cells, and sodium docecyl sulfate [SDS] as an analog) by solution state NMR and CD. We have also quantified the immunomodulatory functions of 1018 by examining its ability to induce chemokine responses ex vivo, its antiendotoxin activity, and its cytotoxicity. Also we have determined the MIC of 1018 required to kill both Gram-positive *Staphylococcus aureus* and Gram-negative *Pseudomonas aeruginosa*. Our findings are compared to those obtained for Bac2A, peptide W3, an A3W substitution of Bac2A and a sequence scrambled version of 1018 (Hilpert et al., 2005), and an inactive peptide from our IDR library, denoted 1019 (Table 1).

Table 1. Antimicrobial Activities of the Peptides Used in This Study

Name	Sequence	MIC (μg/ml) *P. aeruginosa*	MIC (μg/ml) *S. aureus*	Reference
Bac2A	RLARIVVIRVAR	50	17	Hilpert et al. (2005)
W3	RLWRIVVIRVAR	8	2	Hilpert et al. (2005)
1018	VRLIVAVRIWRR	19	5	
1019	IVVWRRQLVKNK	>300	>300	

RESULTS

Chemokine Profile

The immunomodulatory activities of synthetic IDRs are reflected in part by their ability to induce chemokines in PBMCs (Nijnik et al., 2010); previous studies have indicated that this activity is related to their ability to protect against infections (Yu et al., 2009; Cherkasov et al., 2009). Peptide 1018 was therefore tested for its ability to induce responses for the chemokines Gro-α (Figure 1A), MCP-1 (Figure 1B), and MCP-3 (Figure 1C) in human PBMCs. The results demonstrated an 8- to 99-fold increase in chemokine induction at 100 μg/ml and >50-fold at 20 μg/ml as compared with Bac2A and the negative control peptide 1019, whereas W3, a sequence scrambled version of 1018, was only modestly less efficient at chemokine induction. Overall, peptide 1018 exhibited more than 10-fold enhanced chemokine-inducing activities compared with the synthetic peptide IDR-1 (Barlow et al., 2006; Scott et al., 2007) and much greater activities than the (effectively) sequence scrambled parent Bac2A which caused only a 3-fold increase in MCP-1 concentration at 100 μg/ml.

As any immunomodulatory activities of peptides must be tempered with an appreciation for their associated cytotoxicities, 1018 was also tested for host cell toxicity by monitoring hemoglobin release from RBCs as an indicator of loss of cell membrane integrity. At the very high concentration of 375 μg/ml of 1018, only a slight toxic effect was observed with lysis of 14.4% of the red blood cells after 24 hr exposure, while no lytic effect was observed at the concentrations used to demonstrate chemokine induction and no release of lactate dehydrogenase from human PBMCs at concentrations of up to 200 μg/ml, cf. the human cathelicidin LL-37 which demonstrates cytotoxicity at levels above 25–50 μg/ml (Barlow et al., 2006).

Antiendotoxin Activity

Several IDR peptides have been shown to suppress proinflammatory responses in response to the Gram-negative bacteria signature molecule lipopolysaccharide (LPS) (Bowdish et al., 2005b; Mookherjee et al., 2006a, 2006b; Scott et al., 2007).

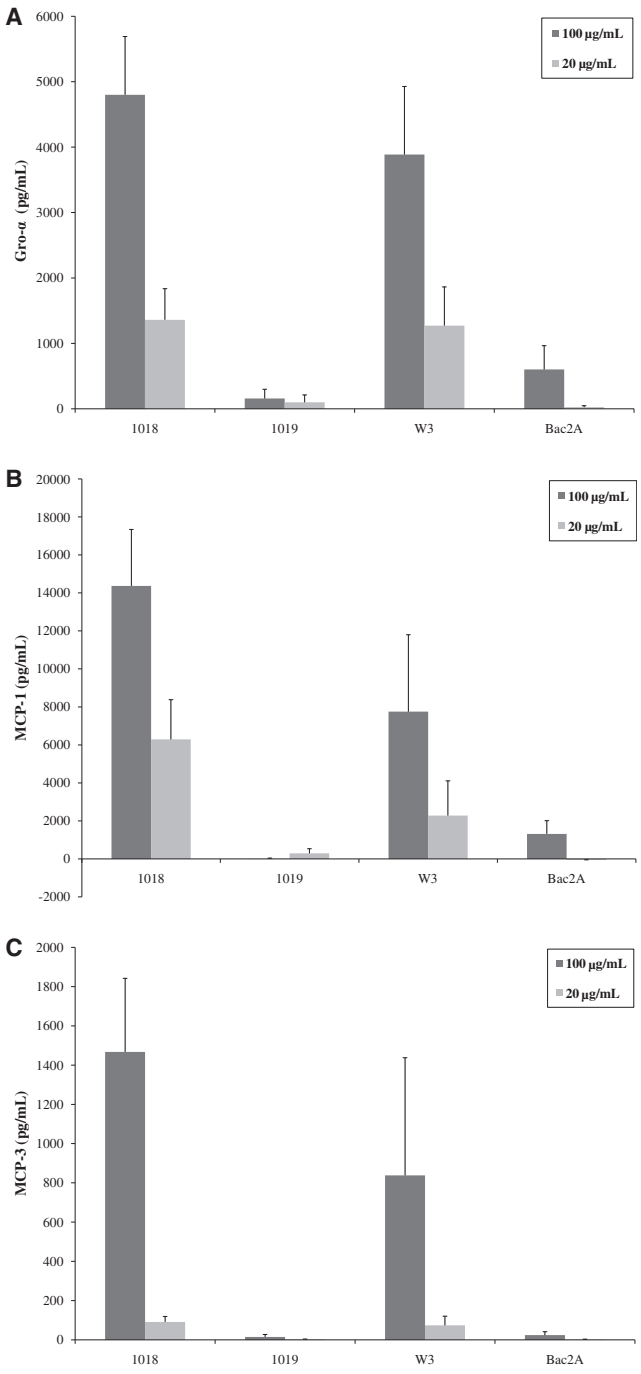

Figure 1. Profile of Relative Fold Change Expression of Gro- α, MCP-1, and MCP-3

(A) Gro-α, (B) MCP-1, and (C) MCP-3 from PBMCs monitored at two concentrations of 20 (light gray) and 100 (dark gray) μg/ml for peptide 1018 (VRLIVAVRIWRR), peptide 1019 (IVVWRRQLVKNK), W3 (RLWRIVVIRVAR), and Bac2A (RLARIVVIRVAR). The results represent mean ± SD of three biological replicates.

Therefore, we determined the potential of 1018 for reducing proinflammatory TNF-α response induced by LPS in human PBMCs. Earlier studies have shown that the induction of TNF-α in response to LPS peaks at 4–8 hr (Scott et al., 2007).

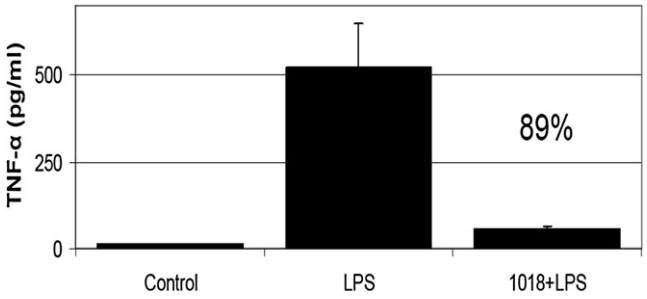

Figure 2. Suppression of LPS-Induced TNF-α in Human Peripheral Blood Mononuclear Cells

PBMCs were incubated with 20 μg/ml of 1018 for 45 min before the addition of 2 ng/ml *P. aeruginosa* LPS or vehicle control. TNF-α secretion was measured after 24 hr incubation at 37°C. The results represent mean ± SD of three biological replicates. Peptide (alone) control gave no significant induction of TNF-α compared with the control (untreated cells); data not shown. The percentage reduction of antiendotoxin activity of 1018 is 89%.

We therefore measured effects of these peptides after 4 hr in the current study.

By itself, 1018 did not demonstrate a significant increase in TNF-α secretion above the background (negative control). However at a concentration of 20 μg/ml, 1018 reduced the LPS-induced TNF-α response by 89% (Figure 2). In contrast at a higher concentration of 50 μg/ml, Bac2A caused only 18% reduction in TNF-α while the scrambled peptide W3 caused only 37% reduction in LPS-stimulated TNF-α production. To determine whether the antiendotoxic response of 1018 was mediated through the direct interaction of the peptides with LPS, the ability of the peptide to directly bind to *P. aeruginosa* LPS was evaluated using a standard dansyl Polymyxin B displacement assay (Fidai et al., 1997; Moore et al., 1991). The peptide displayed no significant binding to LPS (data not shown) indicating that it worked through indirect modulation of proinflammatory responses as suggested in part for LL-37 (Mookherjee et al., 2006a).

Peptide Direct Antibacterial Activity

The immunomodulatory peptide IDR-1 was deliberately designed to exclude any potential antimicrobial activity (Cherkasov et al., 2009). This was not a factor in the design of 1018. Peptide 1018 was screened for activity against both a Gram-negative and Gram-positive bacteria using a modified NCLSA method. The peptide had superior activity to Bac2A, but was less potent than the scrambled peptide W3. Although not particularly potent, 1018 demonstrated a reasonable activity against Gram-positive organism *S. aureus* with an MIC of 5 μg/ml, but was significantly weaker against the Gram-negative *P. aeruginosa* (MIC of 19 μg/ml) (Table 1). The inactive peptide 1019 had MICs of greater than 300 μg/ml for both Gram-positive and Gram-negative organisms used above.

QSAR is an important computational tool in peptide design that seeks to relate physicochemical peptide parameters through descriptors that describe the biological activities of the peptide. Much work has been invested in developing robust QSAR solutions for predicting antimicrobial activity of synthetic peptides (Cherkasov et al., 2009; Nijnik et al., 2010). All of these

approaches require a relatively large number of peptides (a peptide library) to secure a robust model, thus making it difficult to do similar QSAR on the isolated set of peptides described in Table 1. To circumvent this, we used a predictive model of the relationship between antimicrobial activity and peptide structure (reflected through the use of multiple physical chemical and inductive "descriptors") that was built on a library of Bac2A-related peptides (H.J. and R.E.W.H., unpublished data) to predict the activity of Bac2A, W3, and 1018. The model predicted a 2-fold increase in activity between Bac2A and 1018, and between 1018 and W3, matching the observed activities fairly well.

Structure of 1018 in Mammalian Model Membranes

Mammalian cell surface membranes usually comprise largely uncharged lipids. Consequently, a number of structural studies of antimicrobial peptides have used DPC as a model for mammalian membranes. Examples include indolicidin (Rozek et al., 2000), maximin H6 (Kosol and Zangger, 2010), fallaxidin 4.1a (Sherman et al., 2009), and a number of other peptides (Porcelli et al., 2008; for a recent review, see Haney et al., 2009).

CD spectra were recorded for 1018, 1019, Bac2A, and W3 in DPC micelles to determine the structure these peptides adopt in the presence of uncharged lipids. The spectra clearly showed that 1018 adopts an α-helical conformation in this environment (Figure 3B, black), as do Bac2A and W3. A fit of multiple CD spectra using the programs CDSSTR (Johnson, 1999), CONTINLL (Provencher and Glockner, 1981), and SELCON3 (Sreerama et al., 1999; Sreerama and Woody, 1993, 1994) revealed that 70%–98% of peptide 1018 (or 9–12 residues) is helical. W3 and Bac2A also displayed a similar degree of helical content, but the different mean residue ellipticities obtained in the CD spectra of W3 and Bac2A as compared with 1018 suggest that these two peptides did not bind DPC membranes as well as did 1018, or that 1018 interacted in a somewhat more intimate fashion. Recent studies on LL-37 have shown that binding between LL-37 and membranes occurs via the aromatic residue F17 (Porcelli et al., 2008; Wang, 2010). Since Bac2A does not contain a single aromatic residue, this may explain why the interactions between DPC and Bac2A are observed to be weaker. The weak interaction between DPC and W3 (which contains one tryptophan) may be due to the fact that the aromatic residue is located close to the N terminus. In LL-37, the N terminus is more dynamic and less structured that the C terminus (Porcelli et al., 2008). It is worth mentioning that for certain immunomodulatory activities peptides need to translocate into immune cells (Cherkasov et al., 2009; Yu et al., 2009), and we propose that the different ellipticities might reflect propensity to translocate across membranes, a property common to many, but not all, cationic amphipathic peptides rich in arginine residues.

To further quantify the structure of 1018 in DPC micelles, solution state NMR spectra of 1018 in DPC micelles were recorded. Standard homonuclear methods were used to determine the full three-dimensional structure of this peptide (Wuthrich, 1986). Spectra were acquired using total correlation spectroscopy (TOCSY) and nuclear Overhauser enhancement spectroscopy (NOESY) experiments, in phase-sensitive mode using time proportional phase incrementation (TPPI) (Marion and Wuthrich, 1983) in the indirect dimension. A total of 116 unambiguous NOEs were found and used in the structure refinement (see Table S1 available online), using a previously established protocol (Lewis et al., 2007). The large number of *i* to *i+4* and *i* to *i+3* NOE contacts found supported the CD findings (Figure 4A). The resulting family of structures is shown in Figure 4B. The R2 to W10 segment of 1018 was in an α-helical conformation.

Structure of 1018 in Bacterial Model Membranes

Bacterial membranes have varied composition depending on whether the bacteria are Gram-positive or Gram-negative (Epand et al., 2007). In all cases, however, a certain proportion of the lipids contain negatively charged head groups. Therefore, anionic lipids, such as SDS or mixtures of POPE/POPG (Epand et al., 2006) or POPC/POPG are typically used as model bacterial membranes. A number of studies on antimicrobial peptides using these lipids can be found in the literature (Jung et al., 2008; Ramamoorthy et al., 2006) and have been recently reviewed in Haney et al. (2009).

In strong contrast to the structure in DPC micelles, the CD spectra of 1018 in SDS and 1:1 POPC/POPG (Figures 3D and 3E) demonstrated that the peptide adopts a β turn conformation. The spectra for Bac2A and the W3 mutant of Bac2A yielded very similar spectra under the same conditions. Interestingly, the peptide 1019, which displayed no antimicrobial activity, did not adopt any structure in the presence of SDS or POPC/POPG.

Structural Plasticity of 1018

Since the CD data above clearly indicate that 1018 can adopt different conformations in different environments, a local elevation molecular dynamics simulation was run on 1018 to qualitatively determine how easily the peptide could interconvert from one structure to the other. The simulation was run in water, with a starting configuration of a straight α helix. The structures sampled during the course of the simulation are shown in Figure 5 and indicated that the peptide can adopt a range of configurations, some of which are reminiscent of a β turn conformation. Overall, the simulation showed that 1018 rapidly unfolds in water, consistent with the CD data for 1018 in buffer, which indicated that 1018 adopts a random coil conformation under these conditions.

Membrane Perturbation Ability of 1018

Differential scanning calorimetry (DSC) experiments were performed to determine whether 1018 functions by perturbing membrane bilayers. The neutral lipids DMPC and a mixture of 1:1 DMPC/DMPG were chosen as models for mammalian and bacterial membranes, respectively, as used in a number of studies in the literature (Lohner et al., 1999; Pabst et al., 2008). In addition, the lipid DiPoPE was used to examine whether 1018 has the ability to induce membrane curvature (Jung et al., 2008).

The DSC thermograms of 1018 in DMPC alone (Figure S1A), DMPC/DMPG (1:1) (Figure S1B), and DiPoPE (Figure S2) illustrated that this peptide did not significantly perturb model membranes, except at very high (nonphysiological) concentrations. This is in contrast to LL-37 which has been found to induce positive membrane curvature in DiPoPE membranes (Henzler Wildman et al., 2003). This suggests that 1018 most likely

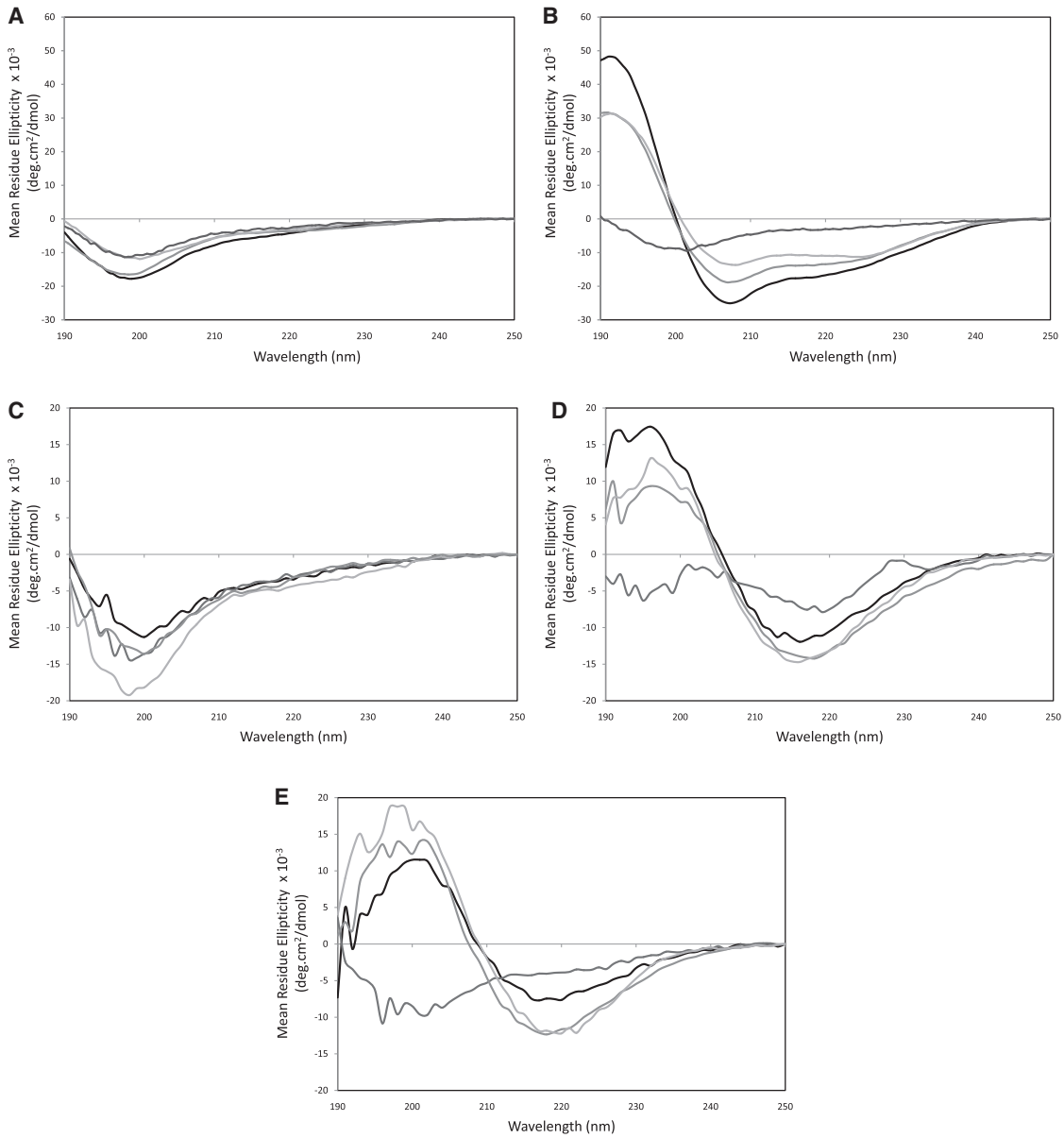

Figure 3. Secondary Structure of 1018, 1019, Bac2A, and W3 from Circular Dichroism

The CD spectra of 1018 (black), 1019 (dark gray), Bac2A (gray), and W3 (light gray) were obtained in (A) phosphate buffer, (B) DPC micelles, (C) 10 mM Tris, (D) in 10 mM SDS micelles (in 10 mM Tris), and (E) 1:1 POPC/POPG vesicles (470 μM) in 10 mM Tris. In (B), 100 μM peptide was mixed with 7.5 mM DPC in 750 μM phosphate buffer (pH 7.3). All peptides are unstructured in buffer alone. Peptide 1019 does not adopt any structure in the presence of DPC, whereas the other three peptides adopt α-helical structure in DPC. In (C)–(E), 0.07 mM of peptide was used. The spectra in (D) and (E) reveal that the peptide 1018 adopts a β turn conformation, as does Bac2A and W3. The peptide 1019 is unstructured in (C)–(E).

functions by translocating across the membrane and perturbing an intracellular target or by some other means (e.g., by interfering with bacterial machineries responsible for producing the cell wall or for performing functions in cell division, energy transduction, or active transport).

DISCUSSION

With the alarming increase in the number of cases of multidrug-resistant bacterial infections such as methicillin-resistant *S. aureus* (MRSA) and vancomycin-resistant enterococci (VRE), it has become important to develop novel anti-infectives. An interesting class of compounds being developed is the cationic host-defense peptides. These peptides are integral components in the defense mechanisms of all living organisms. Interest in the therapeutic potential of HDPs is due to their demonstrated collective ability to kill bacteria by direct antimicrobial action or modulation of host immunity, and their limited induction of bacterial resistance patterns. To date, however, most studies have looked at one or the other of these properties and direct

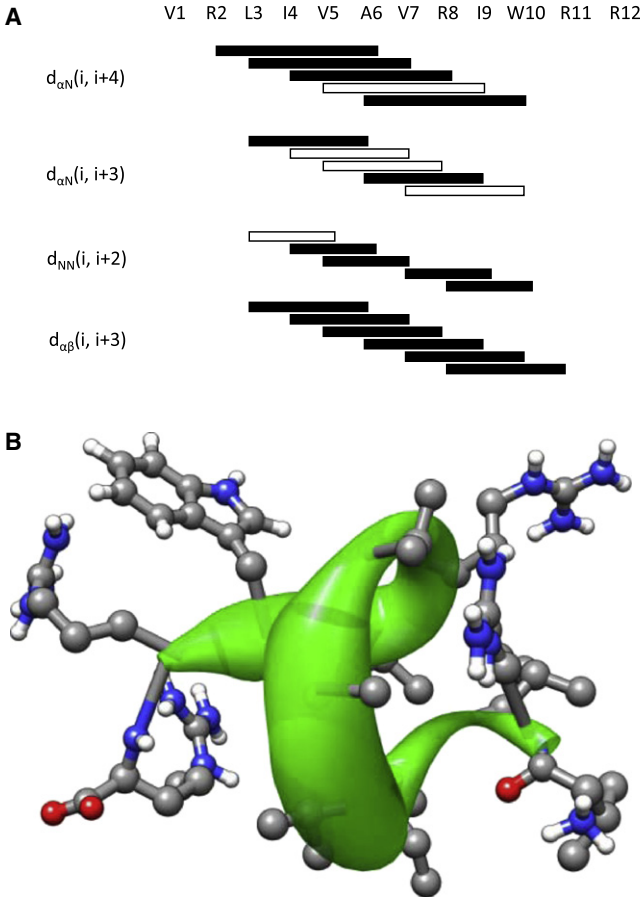

Figure 4. NMR Structure of 1018 in DPC

(A) NOE connectivities observed for 1018. White boxes represent connectivities that may be present, but are overlapped with other resonances.

(B) Representative structure of 1018 determined using NOE refinement. The structure shown is that of the representative structure of cluster 0, the most dominant configuration. The thickness of the worm in green was generated by taking the coordinates of each representative structure of clusters 0..18 and weighting them according to cluster size (see experimental procedure for details).

killing and immunomodulatory properties are being separately exploited in clinical trials (Jenssen and Hancock, 2010).

In this communication, we have investigated the role of structure and function with the peptide 1018, which was one of most potent immunomodulatory peptides obtained from a recently designed library. This peptide was chosen for further study here because, unlike IDR-1 (Scott et al., 2007), it also has moderate antibacterial activity. As the experimental data (Figures 3 and 4) illustrate, and the local elevation simulations (Figure 5) suggest, 1018 is unstructured in water but can adopt different structures in different membrane environments. In model membranes that comprise largely lipids with neutral or zwitterionic head groups, the CD and solution state NMR data showed that 1018 adopted a helical structure. In anionic model membranes, the CD data indicated that 1018 adopted a β turn structure. Interestingly, both Bac2A and W3 also adopted a helical structure in DPC and a β turn structure in SDS and POPC/POPG. In contrast, 1019 did not adopt any structure, be it in buffer, DPC, SDS, or POPC/POPG vesicles.

The peptides that displayed bactericidal activity adopted the same fold in the different environments, despite the fact that their activities are varied, with W3 being the most effective antimicrobial peptide, followed by 1018, and then Bac2A (Table 1). This structural similarity may suggest that the choice of the model membrane is not optimal to gain insight into subtle changes in activity or correspondingly that very small differences in structure can have substantial impacts on activity. Although POPC/POPG is commonly used as a bacterial model membrane (Cheng et al., 2009; Jung et al., 2008; Ramamoorthy et al., 2006; Ramamoorthy, 2009; Su et al., 2008), some studies have suggested that POPE/POPG or other lipid mixtures may be better systems (Chen et al., 2005; Epand and Epand, 2009; Epand et al., 2008; Kline et al., 1987; Salnikov et al., 2008). On the other hand, the strong similarities in amino acid composition of Bac2A, 1018, and W3 may indicate why these three peptides adopt the same structure in an anionic lipid environment, regardless of the exact nature of the lipid head group and the order of the amino acids in the sequence. Alternatively the differences in activity of the active peptides must relate to another property afforded by their different structures and do not reflect just their ability to adopt particular confirmations (although results with 1019 suggest that restructuring in membranes is important). It is worth noting that peptide activities are likely directed by their ability to translocate into cells and/or bind to various targets, and we propose that this is the main feature that differentiates these active peptides.

The immunomodulatory activities of 1018, Bac2A, and W3 were also very different. Bac2A was a very weak inducer of chemokines (Figure 1) and had no practical antiendotoxic activity, consistent with previous studies (Bowdish et al., 2005b). W3, on the other hand, induced substantial expression of MCP-1 at doses of 100 μg/ml but lower than that of 1018 (Figure 1), while antiendotoxic activity was minimal. The CD data showed that all three peptides adopted an α-helical conformation, but differences in the observed mean residue ellipticities (Figure 3B) suggest that the peptides may bind differently to DPC micelles, with 1018 binding the best. This may account for the differences in activity observed. It is also important to note that the differences in immunomodulatory activity may be related to the ability of the peptides to remain monodisperse. Attempts to solve the structure of Bac2A and W3 in detergent DPC micelles (and mixed DPC/SDS micelles) failed because the samples aggregated.

The results with 1019, a poor immunomodulatory and antimicrobial peptide with reasonably strong amino acid compositional relationship to that of the other peptides (but more polar), lend support to the notion that the ability of a peptide to interact with, bind, and translocate through the membranes is an important factor in determining activity. Host-defense peptides (HDPs) are known to be short amphiphilic peptides, with positive side chains interacting with lipid head groups. In both a model of a fully helical structure of 1018 (Figure 6A) and the NMR-derived structure presented in Figure 4B, the positively charged side chains are located on one face of the helix, whereas the hydrophobic residues are on the other. On the other hand, if the structure of the inactive peptide 1019 is modeled as a helix (Figure 6B),

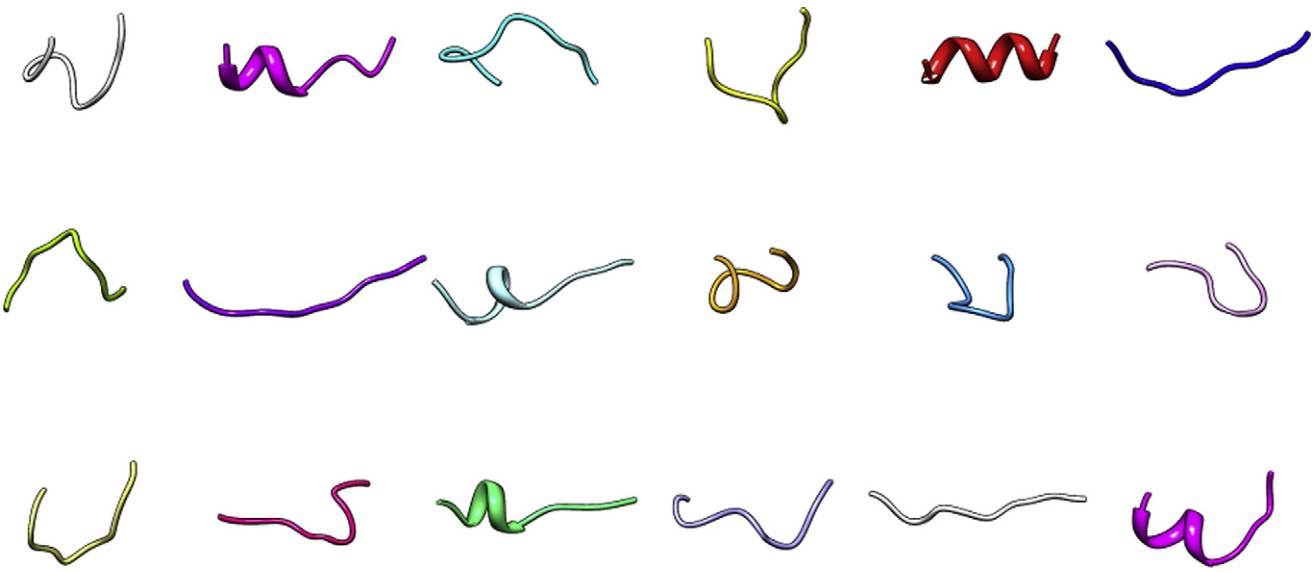

Figure 5. Representative Structures Resulting from a Cluster Analysis of the Free Simulation of 1018 in Water
The structures and their corresponding percentage of occurrence in the simulation are, from left to right, (top row) cluster 0: 30.0%, 1: 10.5%, 2: 10.0%, 3: 9.0%, 4: 5.5%, 5: 4.5%; (middle row) cluster 6: 4.0%, 7: 3.5%, 8,9: 2.5%, 10,11: 2.0%; (bottom row) clusters 12,13: 2.0%, 14–16: 1.5%, 17: 0.5%. The structure starts as a pure helix (cluster 4, shown in red) but rapidly (in ~1 ns, data not shown) unfolds in solution. Some structures are reminiscent of β turns.

the amphipathicity of the peptide is not as pronounced, suggesting a weakened interaction between peptide and membrane bilayer.

Overall, the data presented here suggest that 1018 acts as a direct antimicrobial peptide despite inducing minimal membrane perturbation. This indicates that 1018 translocates in a β turn structure through the membrane to perturb an internal target. When 1018 acts as an immunomodulator, it adopts an α-helical structure. Since it appears that translocation across mammalian membranes is required for chemokine induction (Lau et al., 2005; Mookherjee et al., 2009; Nijnik et al., 2010; Yu et al., 2009), this indicates that the α-helical structure might be optimized for translocation across mammalian membranes, consistent with other studies (Fischer et al., 2000). Interestingly, however, different cell penetrating peptides can adopt different configurations (Deshayes et al., 2004; Magzoub et al., 2001). The ease with which 1018 interconverts between the two structures may be linked to the two functions of 1018 and/or may be required to ensure interaction with targets after the peptide has translocated into cells.

Overall, this manuscript demonstrates that the order and specific nature of amino acids within a peptide sequence determine not only the way they interact with membranes but the downstream consequences of that interaction. This means that quite modest changes (a single A to W substitution going for Bac2A to W3) can have enormous impact, while complete scrambling can be relatively benign (cf. W3 and 1018). Previous studies on Bac2A scrambled peptides have demonstrated that sequence scrambling and single amino acid substitutions can result in peptides that vary from considerably more active to completely inactive with respect to antimicrobial activity (Hilpert et al., 2006). While this considerably complicates informed design of such molecules, the application of QSAR methods to this group of peptides is at least providing predictive methods that can be used to predict function based on structure.

SIGNIFICANCE

We have combined structural and functional studies to demonstrate the link between structure and the ability of 1018 to potently induce chemokine responses, suppress the LPS-induced TNF-α response, and directly kill both Gram-positive and Gram-negative bacteria. We have also demonstrated that QSAR methods can be used to predict function based on the structure of such peptides, but that factors such as the order and the specific nature of amino acids within the peptide sequence need to be considered in the design of molecules that possess both immunomodulatory and antimicrobial activity.

EXPERIMENTAL PROCEDURES

Peptide Synthesis

The peptide 1018 (VRLIVAVRIWRR-$CONH_2$) was synthesized by GenScript (Piscataway, NJ) using solid phase Fmoc chemistry and purified to a purity >95% using reverse phase HPLC. Peptide mass was confirmed by mass spectrometry.

Cell Isolation and Peptide Stimulation

Venous blood from healthy volunteers was collected in Vacutainer collection tubes containing sodium heparin as an anticoagulant (BD Biosciences), in accordance with University of British Columbia ethical approval and guidelines. Blood was diluted with an equal volume of complete RPMI 1640 medium, supplemented with 10% (v/v) heat-inactivated FBS, 2 mM L-glutamine, and 1 mM sodium pyruvate (all from Invitrogen Life Technologies) and separated by centrifugation over a Ficoll-Paque Plus (Amersham Biosciences) density gradient. The buffy coat was collected and washed twice in RPMI 1640 complete medium, and the number of PBMCs was determined by trypan

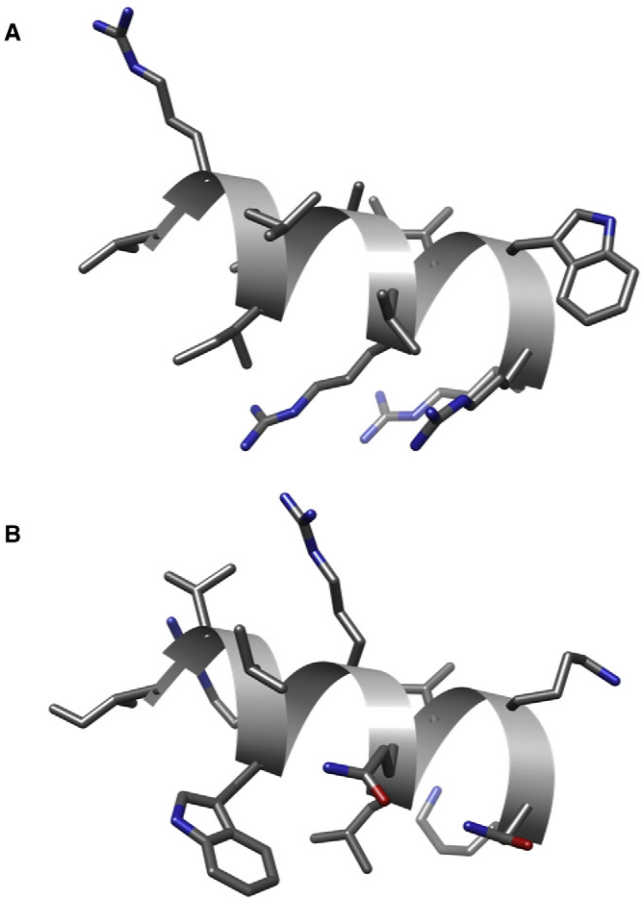

Figure 6. Representative Models of 1018 and 1019
Comparison of a model of (A) 1018 as an α helix and (B) 1019 in the same conformation. The model for 1018 is the starting structure used for the molecular dynamics simulations (red helix in Figure 5). The model for 1019 is generated using the swapaa command in CHIMERA (Pettersen et al., 2004).

blue exclusion. PBMCs (5×10^5) were seeded into 24 well tissue culture dishes (Falcon; BD Biosciences) at 1×10^6 cells/ml at 37°C in 5% CO_2, and rested for 1 hr. The cells were then exposed to peptide at 50 μg/ml for 24 hr. All experiments involved at least three biological replicates.

The red blood cells are left at the bottom of the Ficoll-Paque Plus density gradient. These cells are then pooled together and washed three times in saline and used for hemolysis assay/toxicity testing.

Detection of Chemokines

Following 24 hr of exposure to the peptide, the tissue culture supernatants were centrifuged at 16,000 × g (13,000 rpm) at 4°C for 5 min in an IEC MicroMax centrifuge to obtain cell-free samples. Supernatants were aliquoted and then stored at –20°C before assay for various chemokines. MCP-1, MCP-3, and Gro-α secretion in the tissue culture supernatants were detected by sandwich ELISA kits (BioSource International and eBiosciences, respectively). All assays were performed in triplicate. The concentration of the chemokines in the culture medium was quantified by establishing a standard curve with serial dilutions of the recombinant human MCP-1, MCP-3, or Gro-α, respectively. Secretion of TNF-α was monitored in rested PMBCs and cells were exposed to 20 μg/ml of peptide and/or 2 ng/ml of LPS (*P. aeruginosa*) by capture ELISA after 24 hr (eBiosciences).

Cytotoxicity Assessment

The toxic effect of the peptides was assessed by analyzing their potential for causing hemoglobin release from human red blood cells as a result of cell lysis. The red blood cells were washed three times in sterile 0.85% NaCl (saline) and centrifuged at 500 × g (1500 rpm) for 10 min. Concentrated red blood cells were diluted 1/3 in saline and 150 μl of this cell suspension was mixed with 50 μl of peptide (4.4–251 μM), diluted in a mixture of 0.01% acetic acid, and 0.2% bovine serum albumin (BSA). Triton X-100 (1%) was used as a positive control, demonstrating 100% cell lysis. Sterile saline was used as a negative control. The assay was carried out in 96 well polypropylene microtiter plates (COSTAR Cat. No. 3790). The red blood cells and peptide dilutions were incubated on a rocking table to obtain circulation at 37°C under 5% CO_2 pressure for 24 hr. Light absorbance properties have been monitored at 414 and 546 nm using the ELISA plate reader/spectrophotometer.

PBMCs (2×10^5) were seeded into 96 well plates (Sarstedt, Newton, NC) and incubated at 37°C in 5% CO_2 overnight. The release of cytosolic LDH was then assessed after 24 hr of incubation with peptide 1018 using concentrations up to 200 μg/ml. All experiments were done in triplicate.

Minimal Inhibitory Concentration Determination

The MIC of the peptides was measured using a modified broth microdilution method in Mueller Hinton (MH) medium (MHB, Cat. No. 0757-17-6, DIFCO) (Wiegand et al., 2008). In brief, the peptides were dissolved and stored in glass vials. The assay was performed in sterile 96 well polypropylene microtiter plates (Cat. No. 3790, COSTAR). Serial dilutions of the peptides to be assayed were performed in 0.01% acetic acid (Cat. No. A-38-4, FISHER) containing 0.2% BSA (Cat. No. 735086, Boehringer Mannheim GmbH) at 10× the desired final concentration. Ten microliters of the 10× peptides were added to each well of a 96 well polypropylene plate containing 90 μl of MH media per well. Bacteria obtained from an overnight culture were added to the plate at a concentration of 2–7 × 10^5 CFU/ml and incubated overnight at 37°C. The MIC was taken as the concentration at which no growth was observed.

MIC analysis was done on Gram-negative *P. aeruginosa* PAO1 strain H103 (Hancock and Carey, 1979) and Gram-positive *S. aureus* (ATCC#25923) kindly provided by David Speert (Department of Pediatrics, University of British Columbia). Both tested bacterial strains were categorized as biohazard level 2 pathogens.

CD Spectroscopy

The lipids sodium dodecyl sulfate (SDS), 1-palmitoyl-2-oleoyl-sn-glycero-3-phosphoglycerol (POPC), 1-palmitoyl-2-oleoyl-sn-glycero-3-phosphatidylcholine (POPG), and dodecyl phosphocholine (DPC) were purchased from Avanti Polar Lipids, Inc. (Alabaster, NY). Final sample volumes for CD were 500 μl. POPC/POPG (1:1 molar ratio) and DPC were dissolved with $CHCl_3$ in round-bottomed flasks. The final lipid concentrations were 470 or 1880 μM for POPC/POPG, and 7.5 mM for DPC. $CHCl_3$ was evaporated under a stream of air and the residual solvent was removed under vacuum for at least 12 hr. The dried DPC film was resuspended in 750 μM phosphate buffer [pH 7.4], while POPC/POPG was resuspended in 10 mM Tris buffer [pH 7.4]. For studies with SDS, powdered lipid was dissolved in 10 mM Tris [pH 7.4]. Peptide was weighed and added to the solutions in concentrations of 70 and 100 μM for studies in Tris and phosphate buffers, respectively. All samples were sonicated for at least 30 min in a 40°C water bath and used within 48 hr of preparation.

CD measurements were done on a Jasco J-810 spectropolarimeter equipped with a temperature control unit located at the UBC Laboratories for Molecular Biophysics. Each sample was vortexed for at least 10 s prior to loading into the cuvette. The volume placed in the cuvette (width of 1 mm) was 200 μl. Experiments were done at 35°C with a scan rate of 50 nm/min. The ellipticity was measured every 0.5 nm from 250 to 185 nm. At least three scans per sample were taken and averaged afterward. All CD spectra were baseline corrected by subtracting a blank solvent scan.

NMR Spectroscopy

The NMR sample consisted of 1 mM 1018 in 75 mM DPC, 7.5 mM phosphate buffer, and 8% D_2O (v/v) [pH 7], in a final volume of 600 μl. The sample was sonicated at 40°C for 30 min prior to the start of the NMR experiment.

The spectra were recorded on a Varian Unity500 spectrometer operated by the UBC Laboratory for Molecular Biophysics. Homonuclear TOCSY (spin lock time = 70 ms) (Braunschweiler and Ernst, 1983), NOESY (τ_m = 150 ms) (Jeener et al., 1979), and ROESY (spin lock time = 74 ms) (Bax and Davis, 1985;

Bothner-By et al., 1984) were collected at 40°C. WATERGATE (Piotto et al., 1992) was used for water suppression in this case and the data matrices were 2k by 512. The spectra were referenced to external DSS and processed to yield a 2k × 1k point matrix. The spectra were converted to Bruker format and analyzed using TOPSPIN.

Structure Calculation and Molecular Dynamics Simulations

The GROMOS96 biomolecular simulation package and the 45A3 force field were used (Scott et al., 1999; van Gunsteren et al., 1996). All simulations were performed in explicit SPC water (Berendsen et al., 1981) under rectangular periodic boundary conditions in the NPT ensemble (T = 300 K, p = 1atm) imposed by the Berendsen weak coupling methods (Berendsen et al., 1984). Covalent bonds were constrained using the SHAKE method (Ryckaert et al., 1977) with a relative geometric tolerance of 10^{-4}. A reaction field long-range correction (Tironi et al., 1995) to the truncated Coulomb potential was applied. For the initial coordinates, residues 110–121 were taken from PDB entry 1CWQ (this section is a straight α helix) and modified into the appropriate residue types using CHIMERA (Pettersen et al., 2004). This structure was solvated and minimized, after which the system was rendered neutral by the addition of 4 Cl^- ions. After a second minimization step, initial atomic velocities were generated from a Maxwell-Boltzmann distribution at 300 K and the system was equilibrated for 500 ps with positional restraints on all Cα atoms.

Two separate simulations, each 20 ns in length, were performed starting from this equilibrated system without any positional restraints for data collection. In the first (designated as the "free simulation"), the system was allowed to evolve under its unmodified Hamiltonian. In the second (designated as the "refinement simulation"), the experimentally determined NOE distance restraint (Table S1) data were introduced into the simulation using a time-averaged potential energy function (Torda and van Gunsteren, 1991) with the relaxation time τ_{dr} = 1 ps and force constant K_{dr} = 400 $kJ.mol^{-1}.nm^{-2}$ (Nanzer et al., 1995).

Two hundred configurations, selected at 100 ps time intervals, were selected from the two simulations and subjected to a cluster analysis as previously described (Scott et al., 2006), where the clustering cutoff was set to 0.048 nm (refinement simulation) and 0.135 nm (free simulation) and all Cα atoms were considered in the distance metric.

For the refinement simulation, the cluster analysis resulted in 39 clusters, of which the largest were chosen such that the accumulated percentage is larger than 90% of the sampled 200 structures. This resulted in 19 clusters, labeled 0–18, in decreasing size (cluster 0:36.5%, 1: 20.5%, 2: 5.0%, 3: 5.0%, 4: 4.0%, 5: 4.0%, 6: 2.5%, 7–11: 1.5%, 12–14: 1.0%, 15–18: 0.5%). The representative structure from cluster 0 is shown in Figure 4B.

For the free simulation, the cluster analysis resulted in 28 clusters, of which the largest were chosen such that the accumulated percentage of the sampled 200 structures is larger than 95%. This resulted in 18 clusters, denoted cluster 0–17, the representative structures of which are depicted in Figure 5.

Differential Scanning Calorimetry

1,2-Dimyristoyl-sn-glycero-3-phosphocholine (DMPC), 1,2-dimyristoyl-sn-glycero-3-[phospho-rac-(1-glycerol)] (DMPG), and 1,2-dipalmitoleoyl-sn-glycero-3-phosphoethanolamine (DiPoPE) were purchased from Avanti Polar Lipids, Inc. (Alabaster, NY). All lipids were used as received. For DSC studies in DMPC/DMPG (1:1 molar ratio) and DMPC alone, lipids were dissolved in $CHCl_3$ in round-bottomed flasks. The final lipid concentration was 2.5 mg/ml. $CHCl_3$ was evaporated under a stream of air and residual solvent removed under vacuum for at least 12 hr. The dried lipid films were then resuspended in buffer (20 mM HEPES, 100 mM NaCl [pH 7.0]). Peptide was weighed and added to make three samples with peptide:lipid molar ratios of 1:100, 1:50, and 1:15. The samples were then vortexed vigorously for 30 s and placed in a 45°C water bath for 2 min to bring the temperature above the L_α to H_{II} phase transition temperature. This was repeated two more times to ensure the formation of multilamellar lipid vesicles. Samples were degassed for at least 15 min prior to DSC loading. DSC thermograms were taken on a MicroCal VP-DSC extended range microcalorimeter located at the UBC Center for Biological Calorimetry. The scanning rate was 60°/min with a 15 min prescan using high feedback and a 2 s filter time. The scanning range was 5°–40°C and samples were only scanned once. All scans were baseline corrected by subtracting a buffer scan.

For studies in DiPoPE vesicles, lipid and peptide were codissolved in $CHCl_3$:CH_3OH (2:1 v/v) at a peptide to lipid ratio of 1:250 in a glass test tube. Solvent was evaporated under a stream of air and residual solvent was removed under vacuum for at least 12 hr. The dried film was resuspended in buffer (10 mM Tris, 100 mM NaCl, 1 mM EDTA, 0.002% NaN_3 [pH 7.4]) to give a final lipid concentration of 10 mg/ml. Samples were vortexed vigorously for 30 s with gentle swirling in between; this was repeated twice more to ensure vesicle formation. The L_α to H_{II} phase transition temperatures were recorded using the same calorimeter as before. Two scans were taken from 10°–60°C at a rate of 60°/min with a 15 min prescan using high feedback and a 2 s filter. Only the second scan was deemed suitable for analysis in each case. Buffer thermograms were subtracted for baseline correction.

SUPPLEMENTAL INFORMATION

Supplemental Information includes two figures and one table and can be found with this article online at doi:10.1016/j.chembiol.2010.07.007.

ACKNOWLEDGMENTS

We gratefully acknowledge financial support from the Natural Sciences and Engineering Research Council of Canada (M.W. and S.K.S.), the Canada Foundation for Innovation (for the LMB equipment at UBC used in this study). We also thank the Foundation for the National Institutes of Health and Canadian Institutes for Health Research through the Grand Challenges in Global Health Initiative, and from Genome BC for the Pathogenomics of Innate Immunity research program. REWH was the recipient of a Canada Research Chair. J.K. was supported by a fellowship from the Canadian Cystic Fibrosis Foundation. S.K.S. was a Michael Smith Foundation for Health Research Scholar. This manuscript is dedicated to the memory of Aaron W. J. Wyatt, who tragically passed away on December 24, 2008. Aaron was not only a superb colleague, but also a good friend.

Received: May 13, 2010
Revised: July 3, 2010
Accepted: July 7, 2010
Published: September 23, 2010

REFERENCES

Avrahami, D., and Shai, Y. (2004). A new group of antifungal and antibacterial lipopeptides derived from non-membrane active peptides conjugated to palmitic acid. J. Biol. Chem. *279*, 12277–12285.

Barlow, P.G., Li, Y., Wilkinson, T.S., Bowdish, D.M., Lau, Y.E., Cosseau, C., Haslett, C., Simpson, A.J., Hancock, R.E., and Davidson, D.J. (2006). The human cationic host defense peptide LL-37 mediates contrasting effects on apoptotic pathways in different primary cells of the innate immune system. J. Leukoc. Biol. *80*, 509–520.

Bax, A., and Davis, D.G. (1985). Practical aspects of two-dimensional transverse noe spectroscopy. J. Magn. Reson. *63*, 207–213.

Berendsen, H.J.C., Postma, J.P.M., van Gunsteren, W.F., and Hermans, J. (1981). Interaction models for water in relation to protein hydration. In Intermolecular Forces, B. Pullman, ed. (Dordrecht: Reidel), pp. 331–342.

Berendsen, H.J.C., Postma, J.P.M., van Gunsteren, W.F., Dinola, A., and Haak, J.R. (1984). Molecular-dynamics with coupling to an external Bath. J. Chem. Phys. *81*, 3684–3690.

Bothner-By, A.A., Stephens, R.L., Lee, J., Warren, C.D., and Jeanloz, R.W. (1984). Structure determination of a tetrasaccharide: transient nuclear Overhauser effects in the rotating frame. J. Am. Chem. Soc. *106*, 811–813.

Bowdish, D.M., Davidson, D.J., Lau, Y.E., Lee, K., Scott, M.G., and Hancock, R.E. (2005a). Impact of LL-37 on anti-infective immunity. J. Leukoc. Biol. *77*, 451–459.

Bowdish, D.M., Davidson, D.J., Scott, M.G., and Hancock, R.E. (2005b). Immunomodulatory activities of small host defense peptides. Antimicrob. Agents Chemother. *49*, 1727–1732.

Braunschweiler, L., and Ernst, R.R. (1983). Coherence transfer by isotropic mixing: application to proton correlation spectroscopy. J. Magn. Reson. *53*, 521–528.

Chen, T., Scott, C., Tang, L., Zhou, M., and Shaw, C. (2005). The structural organization of aurein precursor cDNAs from the skin secretion of the Australian green and golden bell frog, Litoria aurea. Regul. Pept. *128*, 75–83.

Cheng, J.T., Hale, J.D., Elliot, M., Hancock, R.E., and Straus, S.K. (2009). Effect of membrane composition on antimicrobial peptides aurein 2.2 and 2.3 from Australian southern bell frogs. Biophys. J. *96*, 552–565.

Cherkasov, A., Hilpert, K., Jenssen, H., Fjell, C.D., Waldbrook, M., Mullaly, S.C., Volkmer, R., and Hancock, R.E. (2009). Use of artificial intelligence in the design of small peptide antibiotics effective against a broad spectrum of highly antibiotic-resistant superbugs. ACS Chem. Biol. *4*, 65–74.

Chertov, O., Yang, D., Howard, O.M., and Oppenheim, J.J. (2000). Leukocyte granule proteins mobilize innate host defenses and adaptive immune responses. Immunol. Rev. *177*, 68–78.

Crovella, S., Antcheva, N., Zelezetsky, I., Boniotto, M., Pacor, S., Verga Falzacappa, M.V., and Tossi, A. (2005). Primate beta-defensins–structure, function and evolution. Curr. Protein Pept. Sci. *6*, 7–21.

Deshayes, S., Heitz, A., Morris, M.C., Charnet, P., Divita, G., and Heitz, F. (2004). Insight into the mechanism of internalization of the cell-penetrating carrier peptide Pep-1 through conformational analysis. Biochemistry *43*, 1449–1457.

Dhople, V., Krukemeyer, A., and Ramamoorthy, A. (2006). The human beta-defensin-3, an antibacterial peptide with multiple biological functions. Biochim. Biophys. Acta *1758*, 1499–1512.

Diamond, G., Russell, J.P., and Bevins, C.L. (1996). Inducible expression of an antibiotic peptide gene in lipopolysaccharide-challenged tracheal epithelial cells. Proc. Natl. Acad. Sci. USA *93*, 5156–5160.

Epand, R.F., Savage, P.B., and Epand, R.M. (2007). Bacterial lipid composition and the antimicrobial efficacy of cationic steroid compounds (Ceragenins). Biochim. Biophys. Acta *1768*, 2500–2509.

Epand, R.F., Schmitt, M.A., Gellman, S.H., and Epand, R.M. (2006). Role of membrane lipids in the mechanism of bacterial species selective toxicity by two alpha/beta-antimicrobial peptides. Biochim. Biophys. Acta *1758*, 1343–1350.

Epand, R.M., and Epand, R.F. (2009). Domains in bacterial membranes and the action of antimicrobial agents. Mol. Biosyst. *5*, 580–587.

Epand, R.M., Rotem, S., Mor, A., Berno, B., and Epand, R.F. (2008). Bacterial membranes as predictors of antimicrobial potency. J. Am. Chem. Soc. *130*, 14346–14352.

Fidai, S., Farmer, S.W., and Hancock, R.E.W. (1997). Interaction of cationic peptides with bacterial membranes. In Methods in Molecular Biology, *Volume 78*, W.M. Shafer, ed. (Totowa, NJ: Humana Press), pp. 187–204.

Fischer, P.M., Zhelev, N.Z., Wang, S., Melville, J.E., Fahraeus, R., and Lane, D.P. (2000). Structure-activity relationship of truncated and substituted analogues of the intracellular delivery vector Penetratin. J. Pept. Res. *55*, 163–172.

Hancock, R.E. (2001). Cationic peptides: effectors in innate immunity and novel antimicrobials. Lancet Infect. Dis. *1*, 156–164.

Hancock, R.E., and Carey, A.M. (1979). Outer membrane of Pseudomonas aeruginosa: heat- 2-mercaptoethanol-modifiable proteins. J. Bacteriol. *140*, 902–910.

Haney, E.F., Hunter, H.N., Matsuzaki, K., and Vogel, H.J. (2009). Solution NMR studies of amphibian antimicrobial peptides: linking structure to function? Biochim. Biophys. Acta *1788*, 1639–1655.

Henzler Wildman, K.A., Lee, D.K., and Ramamoorthy, A. (2003). Mechanism of lipid bilayer disruption by the human antimicrobial peptide, LL-37. Biochemistry *42*, 6545–6558.

Hilpert, K., Elliott, M.R., Volkmer-Engert, R., Henklein, P., Donini, O., Zhou, Q., Winkler, D.F., and Hancock, R.E. (2006). Sequence requirements and an optimization strategy for short antimicrobial peptides. Chem. Biol. *13*, 1101–1107.

Hilpert, K., Volkmer-Engert, R., Walter, T., and Hancock, R.E. (2005). High-throughput generation of small antibacterial peptides with improved activity. Nat. Biotechnol. *23*, 1008–1012.

Hsueh, P.R., Chen, W.H., Teng, L.J., and Luh, K.T. (2005). Nosocomial infections due to methicillin-resistant Staphylococcus aureus and vancomycin-resistant enterococci at a university hospital in Taiwan from 1991 to 2003: resistance trends, antibiotic usage and in vitro activities of newer antimicrobial agents. Int. J. Antimicrob. Agents *26*, 43–49.

Jeener, J., Meier, B.H., Bachmann, P., and Ernst, R.R. (1979). Investigation of exchange processes by two-dimensional NMR spectroscopy. J. Chem. Phys. *71*, 4546–4553.

Jenssen, H., and Hancock, R.E. (2010). Therapeutic potential of HDPs as immunomodulatory agents. Methods Mol. Biol. *618*, 329–347.

Johnson, W.C. (1999). Analyzing protein circular dichroism spectra for accurate secondary structures. Proteins *35*, 307–312.

Jung, D., Powers, J.P., Straus, S.K., and Hancock, R.E. (2008).). Lipid-specific binding of the calcium-dependent antibiotic daptomycin leads to changes in lipid polymorphism of model membranes. Chem. Phys. Lipids. *154*, 120–128.

Kline, M.W., Mason, E.O., Jr., Kaplan, S.L., Lamberth, L.B., and Johnson, G.S. (1987). Comparative in-vitro activity of LY146032 and eight other antibiotics against gram-positive bacteria isolated from children. J. Antimicrob. Chemother. *20*, 203–207.

Kosol, S., and Zangger, K. (2010). Dynamics and orientation of a cationic antimicrobial peptide in two membrane-mimetic systems. J. Struct. Biol. *170*, 172–179.

Lau, Y.E., Rozek, A., Scott, M.G., Goosney, D.L., Davidson, D.J., and Hancock, R.E. (2005). Interaction and cellular localization of the human host defense peptide LL-37 with lung epithelial cells. Infect. Immun. *73*, 583–591.

Lewis, R.N., Liu, F., Krivanek, R., Rybar, P., Hianik, T., Flach, C.R., Mendelsohn, R., Chen, Y., Mant, C.T., Hodges, R.S., and McElhaney, R.N. (2007). Studies of the minimum hydrophobicity of α-helical peptides required to maintain a stable transmembrane association with phospholipid bilayer membranes. Biochemistry *46*, 1042–1054.

Lohner, K., Staudegger, E., Prenner, E.J., Lewis, R.N., Kriechbaum, M., Degovics, G., and McElhaney, R.N. (1999). Effect of staphylococcal delta-lysin on the thermotropic phase behavior and vesicle morphology of dimyristoylphosphatidylcholine lipid bilayer model membranes. Differential scanning calorimetric, 31P nuclear magnetic resonance and Fourier transform infrared spectroscopic, and X-ray diffraction studies. Biochemistry *38*, 16514–16528.

Magzoub, M., Kilk, K., Eriksson, L.E., Langel, U., and Graslund, A. (2001). Interaction and structure induction of cell-penetrating peptides in the presence of phospholipid vesicles. Biochim. Biophys. Acta *1512*, 77–89.

Marion, D., and Wuthrich, K. (1983). Application of phase sensitive two-dimensional correlated spectroscopy (COSY) for measurements of 1H-1H spin-spin coupling constants in proteins. Biochem. Biophys. Res. Commun. *113*, 967–974.

Mookherjee, N., Brown, K.L., Bowdish, D.M., Doria, S., Falsafi, R., Hokamp, K., Roche, F.M., Mu, R., Doho, G.H., Pistolic, J., et al. (2006a). Modulation of the TLR-mediated inflammatory response by the endogenous human host defense peptide LL-37. J. Immunol. *176*, 2455–2464.

Mookherjee, N., Wilson, H.L., Doria, S., Popowych, Y., Falsafi, R., Yu, J.J., Li, Y., Veatch, S., Roche, F.M., Brown, K.L., et al. (2006b). Bovine and human cathelicidin cationic host defense peptides similarly suppress transcriptional responses to bacterial lipopolysaccharide. J. Leukoc. Biol. *80*, 1563–1574.

Mookherjee, N., Lippert, D.N., Hamill, P., Falsafi, R., Nijnik, A., Kindrachuk, J., Pistolic, J., Gardy, J., Miri, P., Naseer, M., et al. (2009). Intracellular receptor for human host defense peptide LL-37 in monocytes. J. Immunol. *183*, 2688–2696.

Moore, K.S., Bevins, C.L., Brasseur, M.M., Tomassini, N., Turner, K., Eck, H., and Zasloff, M. (1991). Antimicrobial peptides in the stomach of Xenopus laevis. J. Biol. Chem. *266*, 19851–19857.

Mygind, P.H., Fischer, R.L., Schnorr, K.M., Hansen, M.T., Sonksen, C.P., Ludvigsen, S., Raventos, D., Buskov, S., Christensen, B., De Maria, L., et al. (2005). Plectasin is a peptide antibiotic with therapeutic potential from a saprophytic fungus. Nature *437*, 975–980.

Nanzer, A.P., van Gunsteren, W.F., and Torda, A.E. (1995). Parametrization of time-averaged distance restraints in Md simulations. J. Biomol. NMR *6*, 313–320.

Nijnik, A., Madera, L., Ma, S., Waldbrook, M., Elliott, M.R., Easton, D.M., Mayer, M.L., Mullaly, S.C., Kindrachuk, J., Jenssen, H., and Hancock, R.E.W. (2010). Synthetic cationic peptide IDR-1002 provides protection against bacterial infections through chemokine induction and enhanced leukocyte recruitment. J. Immunol. *184*, 2539–2550.

Pabst, G., Grage, S.L., Danner-Pongratz, S., Jing, W., Ulrich, A.S., Watts, A., Lohner, K., and Hickel, A. (2008). Membrane thickening by the antimicrobial peptide PGLa. Biophys. J. *95*, 5779–5788.

Pettersen, E.F., Goddard, T.D., Huang, C.C., Couch, G.S., Greenblatt, D.M., Meng, E.C., and Ferrin, T.E. (2004). UCSF Chimera–a visualization system for exploratory research and analysis. J. Comput. Chem. *25*, 1605–1612.

Piotto, M., Saudek, V., and Sklenar, V. (1992). Gradient-tailored excitation for single-quantum NMR spectroscopy of aqueous solutions. J. Biomol. NMR *2*, 661–665.

Porcelli, F., Buck-Koehntop, B.A., Thennarasu, S., Ramamoorthy, A., and Veglia, G. (2006). Structures of the dimeric and monomeric variants of magainin antimicrobial peptides (MSI-78 and MSI-594) in micelles and bilayers, determined by NMR spectroscopy. Biochemistry *45*, 5793–5799.

Porcelli, F., Verardi, R., Shi, L., Henzler-Wildman, K.A., Ramamoorthy, A., and Veglia, G. (2008). NMR structure of the cathelicidin-derived human antimicrobial peptide LL-37 in dodecylphosphocholine micelles. Biochemistry *47*, 5565–5572.

Provencher, S.W., and Glockner, J. (1981). Estimation of globular protein secondary structure from circular dichroism. Biochemistry *20*, 33–37.

Ramamoorthy, A. (2009). Beyond NMR spectra of antimicrobial peptides: dynamical images at atomic resolution and functional insights. Solid State Nucl. Magn. Reson. *35*, 201–207.

Ramamoorthy, A., Thennarasu, S., Lee, D.K., Tan, A., and Maloy, L. (2006). Solid-state NMR investigation of the membrane-disrupting mechanism of antimicrobial peptides MSI-78 and MSI-594 derived from magainin 2 and melittin. Biophys. J. *91*, 206–216.

Rehaume, L.M., and Hancock, R.E. (2008). Neutrophil-derived defensins as modulators of innate immune function. Crit. Rev. Immunol. *28*, 185–200.

Rozek, A., Friedrich, C.L., and Hancock, R.E. (2000). Structure of the bovine antimicrobial peptide indolicidin bound to dodecylphosphocholine and sodium dodecyl sulfate micelles. Biochemistry *39*, 15765–15774.

Ryckaert, J.P., Ciccotti, G., and Berendsen, H.J.C. (1977). Numerical-integration of cartesian equations of motion of a system with constraints—molecular-dynamics of N-alkanes. J. Comput. Phys. *23*, 327–341.

Sahl, H.G., Pag, U., Bonness, S., Wagner, S., Antcheva, N., and Tossi, A. (2005). Mammalian defensins: structures and mechanism of antibiotic activity. J. Leukoc. Biol. *77*, 466–475.

Salnikov, E.S., Friedrich, H., Li, X., Bertani, P., Reismann, S., Hertweck, C., O'Neil, J.D., Raap, J., and Bechinger, B. (2008). Structure and alignment of the membrane-associated peptaibols ampullosporin A and alamethicin by oriented 15N and 31P solid-state NMR spectroscopy. Biophys. J. *96*, 86–100.

Scott, W.R.P., Hunenberger, P.H., Tironi, I.G., Mark, A.E., Billeter, S.R., Fennen, J., Torda, A.E., Huber, T., Kruger, P., and van Gunsteren, W.F. (1999). The GROMOS biomolecular simulation program package. J. Phys. Chem. A *103*, 3596–3607.

Scott, W.R., Seo, E., Huttunen, H., Wallhorn, D., Sherman, J.C., and SK, S. (2006). Characterization of de novo four-helix bundles by molecular dynamics simulations. Proteins *64*, 719–729.

Scott, M.G., Dullaghan, E., Mookherjee, N., Glavas, N., Waldbrook, M., Thompson, A., Wang, A., Lee, K., Doria, S., Hamill, P., et al. (2007). An anti-infective peptide that selectively modulates the innate immune response. Nat. Biotechnol. *25*, 465–472.

Sherman, P.J., Jackway, R.J., Gehman, J.D., Praporski, S., McCubbin, G.A., Mechler, A., Martin, L.L., Separovic, F., and Bowie, J.H. (2009). Solution structure and membrane interactions of the antimicrobial peptide fallaxidin 4.1a: an NMR and QCM study. Biochemistry *48*, 11892–11901.

Sitaram, N., Sai, K.P., Singh, S., Sankaran, K., and Nagaraj, R. (2002). Structure-function relationship studies on the frog skin antimicrobial peptide tigerinin 1: design of analogs with improved activity and their action on clinical bacterial isolates. Antimicrob. Agents Chemother. *46*, 2279–2283.

Sreerama, N., and Woody, R.W. (1993). A self-consistent method for the analysis of protein secondary structure from circular dichroism. Anal. Biochem. *209*, 32–44.

Sreerama, N., and Woody, R.W. (1994). Protein secondary structure from circular dichroism spectroscopy. Combining variable selection principle and cluster analysis with neural network, ridge regression and self-consistent methods. J. Mol. Biol. *242*, 497–507.

Sreerama, N., Venyaminov, S.Y., and Woody, R.W. (1999). Estimation of the number of α-helical and beta-strand segments in proteins using circular dichroism spectroscopy. Protein Sci. *8*, 370–380.

Straus, S.K., and Hancock, R.E. (2006). Mode of action of the new antibiotic for Gram-positive pathogens daptomycin: comparison with cationic antimicrobial peptides and lipopeptides. Biochim. Biophys. Acta *1758*, 1215–1223.

Strömstedt, A.A., Pasupuleti, M., Schmidtchen, A., and Malmsten, M. (2009). Evaluation of strategies for improving proteolytic resistance of antimicrobial peptides by using variants of EFK17, an internal segment of LL-37. Antimicrob. Agents Chemother. *53*, 593–602.

Su, Y., Mani, R., Doherty, T., Waring, A.J., and Hong, M. (2008). Reversible sheet-turn conformational change of a cell-penetrating peptide in lipid bilayers studied by solid-state NMR. J. Mol. Biol. *381*, 1133–1144.

Tironi, I.G., Sperb, R., Smith, P.E., and van Gunsteren, W.F. (1995). A generalized reaction field method for molecular-dynamics simulations. J. Chem. Phys. *102*, 5451–5459.

Torda, A.E., and van Gunsteren, W.F. (1991). The refinement of Nmr structures by molecular-dynamics simulation. Comput. Phys. Commun. *62*, 289–296.

van Gunsteren, W.F., Billeter, S.R., Eising, A.A., Huenenberger, P.H., Krueger, P., Mark, A.E., Scott, W.R.P., and Tironi, I.G. (1996). Biomolecular simulation: the GROMOS96 manual and user guide. (Zurich, Groningen: VdF: Hochschulverlag AG an der ETH Zurich BIOMOS b.v.).

Wang, G. (2010). Structure, dynamics and mapping of membrane-binding residues of micelle-bound antimicrobial peptides by natural abundance (13)C NMR spectroscopy. Biochim. Biophys. Acta *1798*, 114–121.

Wiegand, I., Hilpert, K., and Hancock, R.E. (2008). Agar and broth dilution methods to determine the minimal inhibitory concentration (MIC) of antimicrobial substances. Nat. Protoc. *3*, 163–175.

Wu, M., and Hancock, R.E. (1999a). Improved derivatives of bactenecin, a cyclic dodecameric antimicrobial cationic peptide. Antimicrob. Agents Chemother. *43*, 1274–1276.

Wu, M., and Hancock, R.E. (1999b). Interaction of the cyclic antimicrobial cationic peptide bactenecin with the outer and cytoplasmic membrane. J. Biol. Chem. *274*, 29–35.

Wuthrich, K. (1986). NMR of Proteins and Nucleic Acids (New York: Wiley).

Yu, H.B., Kielczewska, A., Rozek, A., Takenaka, S., Li, Y., Thorson, L., Hancock, R.E., Guarna, M.M., North, J.R., Foster, L.J., et al. (2009). Sequestosome-1/p62 is the key intracellular target of innate defense regulator peptide. J. Biol. Chem. *284*, 36007–36011.

Zasloff, M. (2002). Antimicrobial peptides of multicellular organisms. Nature *415*, 389–395.

Zhang, G., Wu, H., Ross, C.R., Minton, J.E., and Blecha, F. (2000a). Cloning of porcine NRAMP1 and its induction by lipopolysaccharide, tumor necrosis factor alpha, and interleukin-1beta: role of CD14 and mitogen-activated protein kinases. Infect. Immun. *68*, 1086–1093.

Zhang, L., Dhillon, P., Yan, H., Farmer, S., and Hancock, R.E. (2000b). Interactions of bacterial cationic peptide antibiotics with outer and cytoplasmic membranes of Pseudomonas aeruginosa. Antimicrob. Agents Chemother. *44*, 3317–3321.

